Classification.

Primary: Biological Sciences: Ecology
Secondary: Physical Sciences: Engineering

Passive energy recapture in jellyfish contributes to propulsive advantage over other metazoans

Brad J. Gemmell[1, 2], John H. Costello[1, 2], Sean P. Colin[1, 3], Colin J. Stewart[4], John O. Dabiri[5], Danesh Tafti[4], Shashank Priya[4]

[1] Marine Biological Laboratory, Woods Hole, MA 02543.
[2] Providence College, Providence RI 02908.
[3] Roger Williams University, Bristol, RI 02809.
[4] Virginia Tech, Blacksburg, VA 24061.
[5] California Institute of Technology, Pasadena, CA 91106.

Corresponding author:

Brad Gemmell
bgemmell@mbl.edu
Marine Biological Laboratory
7 MBL St
Woods Hole, MA
02543
512-983-0244

Abstract

Gelatinous zooplankton populations are well known for their ability to take over perturbed ecosystems. The ability of these animals to outcompete and functionally replace fish that exhibit an effective visual predatory mode is counterintuitive because jellyfish are described as inefficient swimmers that must rely on direct contact with prey in order to feed. We show that jellyfish exhibit a novel mechanism of passive energy recapture, which is exploited to allow jellyfish to travel 30 percent further each swimming cycle, thereby reducing metabolic energy demand by swimming muscles. By accounting for large interspecific differences in net metabolic rates, we demonstrate, contrary to prevailing views, the jellyfish (*Aurelia aurita*) is one of the most energetically efficient propulsors on the planet, exhibiting a cost-of-transport (J kg^{-1} m^{-1}) lower than other metazoans. We estimate that reduced metabolic demand by passive energy recapture improves cost-of-transport by 48%, allowing jellyfish to achieve the large sizes required for sufficient prey encounters. Pressure calculations, using both computational fluid dynamics (CFD) and a new method from empirical velocity field measurements demonstrate that this extra thrust results from positive pressure created by a vortex ring underneath the bell during the refilling phase of swimming. These results demonstrate a physical basis for the ecological success of medusan swimmers despite their simple body plan. Results from this study also have implications for bio-inspired design where low-energy propulsion is required.

Significance statement:

Jellyfish have the ability to bloom and take over perturbed ecosystems but this is counterintuitive because jellyfish are described as inefficient swimmers and rely on direct contact with prey in order to feed. To understand how jellyfish can outcompete effective visual hunters such as fish, we investigate energetics of propulsion. We find that jellyfish exhibit a novel mechanism of passive energy recapture, which can reduce metabolic energy demand by swimming muscles. Contrary to prevailing views, this contributes to jellyfish being one of the most energetically efficient propulsors on the planet. These results demonstrate a physical basis for the ecological success of medusan swimmers despite their simple body plan and have implications for bio-inspired design where low-energy propulsion is required.

/body **Introduction.** During jellyfish swimming, acceleration is achieved in the contraction phase, whereas peak drag and deceleration occur in the relaxation phase. Thus, studies investigating the propulsion of jellyfish have primarily focused on the contraction phase (1-4). Potential advantages in swimming efficiency of gelatinous zooplankton locomotion have been previously overlooked because efficiency of swimming is commonly estimated using the Froude number (E_f) (5-7), a metric originally designed to quantify the propulsive performance of ships. E_f is defined as the ratio of useful power produced during locomotion to the useful power plus the power lost to the fluid (8). It has been used to compare biological species of different sizes and morphology. Previous work describes jellyfish as inefficient swimmers with E_f values of

0.09-0.53 (5), compared to ≈0.8 in fish (9, 10). However, this method, does not account for large interspecific differences in the net metabolic energy demand of swimming, and there is no protocol for including the relaxation phase of pulsating swimmers in such a calculation (11).

A more comprehensive and ecologically relevant method of estimating energetic costs of locomotion is the net cost-of-transport (COT) analysis (Fig 1a, d). COT is defined as: $\frac{Energy}{Mass \times Velocity_{avg}}$ and is a suitable metric for interspecific comparisons of swimming efficiency because the energetic expenditures for generating kinematic and fluid motion are not constant among species (Fig 1b, c). By this measure, the moon jellyfish, *Aurelia aurita*, expends significantly less energy per unit of wet mass per unit distance travelled than other animals. The ability exhibit a low COT has also been reported in another jellyfish species (*Stomolophus meleagris*) (12).

How can jellyfish swim with such a low COT and how do jellyfish species (*Aurelia* and *Stomolophus*) compare to each other and to fish? Using the salmon (*Oncorhynchus nerka*), another efficient swimmer as a reference, we show that net COT is ≥3.5 times greater for salmon and ≥2 times greater for *Stomolophus* relative to *Aurelia* (Fig 1d). The lower COT for *Aurelia* is primarily a function of its low net metabolic rate for swimming, which is 15 times lower than that of *Stomolophus* (Fig 1c).

Medusae can exhibit such low respiration rates due to the large proportion of metabolically inactive tissue during swimming. Jellyfish have low body carbon relative to other swimmers (13), which results in ≤1% of the body mass represented by muscle (12, 14). Fish, in comparison, have a body mass in which is ≥50% muscle (15). Expending such little energy to generate propulsive thrust is an adaptive advantage for gelatinous zooplankton. However, consider the tradeoff. Low body carbon and muscle mass limits propulsive options for jellyfish (16). Swimming proficiency is sacrificed because low muscle mass in gelatinous zooplankton restricts them to low velocities and burst swimming velocities are only 30% greater than that of routine swimming (12). Low velocities typically increase COT but in jellyfish this is more than compensated for by low metabolic demand.

While low muscle mass limits the thrust jellyfish can produce during contraction (16, 17), we show that jellyfish use a form of passive energy recapture to enhance their swimming and further reduce their COT. Contraction of the bell generates a starting vortex at the bell margin and a

stopping vortex with opposite-sign vorticity forms upstream of the starting vortex (11). After shedding of the starting vortex, the relaxation or refilling phase begins and enhances stopping vortex circulation and vorticity while drawing the fluid under the bell (Fig 2a, Video S1). While medusae exhibit greater accelerations and peak velocities during contraction, peak circulation of the stopping vortex (which is proportional to the thrust generated) can be significantly greater (ANOVA, $n = 10$, $P = 0.01$) than the starting vortex (Fig 2a), illustrating the potential importance of stopping vortices during swimming. A study using computational fluid dynamics (CFD) has previously demonstrated that power can be generated during the refilling (relaxation) phase (18) but relative contributions to efficiency and distance are unknown.

The mesogleal tissue of jellyfish has both viscoelastic (19) and elastic properties (20). However, the refilling phase, responsible for the secondary thrust, is found to be powered exclusively from the elastic properties of mesoglea (20) (Fig S2). The stress-strain relationship within this elastic tissue exhibits a non-linear, J-shaped relationship (21, 22). This allows the tissue to strain easily at the beginning of the contraction when potential for hydrodynamic output is high and store most strain energy near the end of the contraction. This can aid in optimizing energetic efficiency because during periods of acceleration nearly all energy is devoted to thrust generation while elastic strain storage occurs mostly at the end of the contraction cycle. Therefore, the large stopping vortex is produced and positioned under the bell using only stored strain energy and no additional energy from antagonistic muscle groups. An examination of multiple jellyfish species demonstrates that this translates to only a small proportion of each swimming cycle in jellyfish (approximately 20%) requiring muscle contraction (Fig 3a-c). The energy required to decelerate the contracting bell is translated to refilling the bell, similar to the mechanism demonstrated in flying insects which greatly reduces energetic costs for thrust production (23).

Our results show that 32% (SD 0.6%) of the total distance travelled per pulse can occur during the post-relaxation period (inter-pulse phase) where the animal produces no kinematic motion (i.e. coasting) and after inertial motion would have ceased (Fig 2b, c). Anesthetized *A. aurita* were artificially propelled forward at natural swimming velocities to allow observation of the stopping vortex influence beyond the duration at which the subsequent contraction normally begins. We show that passive bell refilling can produce thrust for an extended period after bell motion ceases (Fig S1). The force produced can carry a 4cm *Aurelia* an additional 10.1mm (SD

0.8, n=4) each pulse, which is 80% of the measured 12.7 mm (SD 3.5, n=5) achieved during the kinematically active portion of normal swimming.

To elucidate how thrust is generated after refilling of the bell, we measured pressure around the body of the jellyfish using a combination of computational fluid dynamics (CFD) and a newly developed empirical technique for pressure estimation from velocity field measurements. Oblate medusae are known to produce more complex pressure fields at the subumbrellar surface relative to jetting medusae (24). We find that during bell relaxation the pressure is typically low as refilling occurs, but subsequently induced flow from the stopping vortex builds against the subumbrellar surface and creates a large region of positive pressure between the low pressure cores of the vortex ring (Fig 4, Video S2). The resulting high pressure creates enough force to cause an additional acceleration of the body after initial contraction and prior to the next cycle (Fig 4b, c).

A simple, conservative estimate can be made to understand how passive energy recapture contributes to COT in *Aurelia*. Eliminating the inter-pulse duration (and thus any influence of passive energy recapture) will result in doubling of the pulse frequency as: $\frac{T_{ip}}{T_{tot}}$ = 0.50 (SD 0.05, n=20), where T_{ip} is the time of the inter-pulse duration and T_{tot} is the total time of each pulse. While the relationship between pulse frequency and respiration is unknown for jellyfish, it is exponential for fish (25). Conservatively, we assume a linear relationship between respiration rate and pulse frequency. By applying the measured velocity during the active phase (V_A) of the swimming cycle over the total velocity (V_T) for animals 2-10 cm in diameter (V_A/V_T = 1.35 n=12), we find that COT will increase at least by: $\frac{2\text{Energy}}{\text{Mass}(1.35\text{Velocity})}$ = 1.48 times, or 48% in *Aurelia* if passive energy recapture is not used.

While cnidarian swimming muscle structure and force production resembles that of other animal groups (16), the cnidarian muscle fibers are housed solely within epitheliomuscular cells. This single-cell layer limits the thickness of swimming muscles within cnidarians and thus, force production during medusan swimming. Therefore, beyond a certain size, and unlike other animals, jellyfish do not continue to increase swimming velocity with size. As a result, the additional force required to continue increasing swimming speed with body size is limited to a specific range in jellyfish. This has consequences with respect to COT as jellyfish appear to have

the greatest advantage over other metazoans when they are small. However, extrapolating the results from Figure 1 indicates fish only begin to exhibit a lower COT than *Aurelia* beyond a body mass of approximately 100kg.

The ability of jellyfish to utilize passive energy recapture reduces metabolic demand while increasing fluid (thus prey) encountered by feeding structures and translates to more energy available for growth and reproduction. Such energetic advantages would enable jellyfish populations to exploit environments with excess prey and contribute to the demonstrated ability of some jellyfish species to bloom rapidly over short periods and outcompete species such as fish (26). Our results show that since COT can vary by more than twofold in jellyfish alone, the species-specific influence of passive energy recapture should be taken into account when trying to understand bloom dynamics and trophic competition. In addition, the passive energy recapture demonstrated in *Aurelia* may be an important consideration in biomimetic design where low-energy demands are required for efficient vehicle design. The fact that passive energy recapture appears to scale well with animal size also suggests there are important design implications to be explored over a wide range of size scales.

Methods

Swimming Kinematics. Free-swimming jellyfish (1.5-6cm) were recorded in a glass filming vessel (30x10x25cm) by a high speed digital video camera (Fastcam 1024 PCI; Photron) at 1,000 frames s^{-1}. Only recordings of animals swimming upwards were used in the analysis to eliminate the possibility of gravitational force from aiding forward motion of the animal between pulses. Detailed swimming kinematics (2D) were obtained using Image J v1.46 software to track the x and y coordinates of the apex of the jellyfish bell and the tips of the bell margin over time. Swimming speed was calculated from the change in the position of the apex over time as:

$$U = \frac{((x_2 - x_1)^2 + (y_2 - y_1)^2)^{1/2}}{t_2 - t_1} \quad (1)$$

Jellyfish were illuminated with a laser sheet (LaVision 2W continuous wave; 680 nm) oriented perpendicular to the camera's optical axis to provide a distinctive body outline for image analysis and to ensure the animal remained in plane which assures accuracy of 2D estimates of position and velocity. Swimming kinematics of large (>6cm) *Aurelia aurita* were obtained using a high

definition Sony HDV Handycam (model HDR-FX1) at a dedicated off-exhibit tank at the New England Aquarium. Here, a 500 mW laser (Laserglow Hercules series 432 nm) was formed into a thin sheet to illuminate (from above) the outline of the animal for kinematic analysis.

Cost-of-Transport. The metabolic cost-of-transport (COT) per unit mass and distance (J Kg^{-1} m^{-1}) for the moon jellyfish (*Aurelia aurita*) was estimated from mass specific swimming speeds and respiration rates. Mass specific swimming speeds were obtained from kinematic data (current study) and supplemented with data from (27, 28). Mass specific active respiration data for *A. aurita* was obtained from (29). Conversion of metabolic respiration to energy expended (Joules) is accomplished by using the conversion factor of 19 J $mL^{-1}O_2$ (12).To obtain net COT, which accounts only for energy expended toward locomotion, basal energy consumption must be subtracted from the active rates. Because basal rates are found to be half the active rates in medusae (12), we calculate the proportion of energy dedicated to location in *Aurelia* as 0.5 times the active rate. It should be noted that this makes our net $COT_{Aurelia}$ estimates conservative, because pulsation rates in *Aurelia* are lower than species that were studied (12). This is because *Aurelia* spends proportionally less time actively contracting compared many other species (see Fig S1), and since this is the only time energy is expended for swimming, due to passive relaxation (19), the proportion of the active to total metabolic rate in *Aurelia* (and COT) will likely be lower. The mass specific respiration and swimming data for salmon (30) was used for comparative purposes.

Net COT was calculated using the equation:

$$COT_{Net} = \frac{Energy_{swim}}{Mass \times Velocity} \quad (2)$$

Net COT for runners, fliers and other swimmers were obtained and re-plotted from (12, 29, 30), using GetData v2.25 graph digitizing software.

Fluid Properties Around Swimming Jellyfish. Fluid motion created by the jellyfish while swimming was quantified using 2D Digital Particle Image Velocimetry (DPIV). Using the setup described above, the filtered seawater was seeded with 10-µm hollow glass beads. The velocities of particles illuminated in the laser sheet were determined from sequential images analyzed using a cross-correlation algorithm (LaVision Software). Image pairs were analyzed with shifting

overlapping interrogation windows of decreasing size of 64 × 64 pixels to 32 × 32 pixels or 32x32 pixels to 16x16 pixels. For details on circulation and pressure estimates, see online SI.

Kinematic data was log transformed and checked for normality using a Shapiro–Wilks test. Data was subsequently tested using a one-way analysis of variance (ANOVA) to determine if a significant difference existed between means.

CFD Model of a Swimming Jellyfish. We developed a jellyfish model using the bell kinematics of an individual 3 cm diameter, free-swimming moon jellyfish (*Aurelia aurita*). Digitized points along this half were spatially interpolated using 8th-order polynomials, temporally smoothed using a Butterworth filter, and temporally interpolated using cubic-spline polynomials.

The ANSYS Fluent 13.0 commercial package was used to solve the unsteady, incompressible, axisymmetric Navier-Stokes equations. Swimming was modeled by coupling the forward motion of the jellyfish to the hydrodynamic forces exerted on the bell. Pressure and shear forces acting in the axial direction were integrated across the jellyfish surface at the end of each time step and the resulting body acceleration was calculated. The discrete form of this force balance is given by the equation:

$$\sum {F_z}^n = m\left(\frac{d^2z}{dt^2}\right)^n \quad (3)$$

where $\sum {F_z}^n$ is the sum of all pressure and shear forces in the axial direction at time step n, m is the mass of the jellyfish (density assumed to be the same as the surrounding water: ρ = 998.2 kg m^{-3}) , and $\left(\frac{d^2z}{dt^2}\right)^n$ is the axial acceleration at the center of mass of the jellyfish. Using Taylor series expansions, the acceleration can be approximated by a second order accurate, backward finite difference equation:

$$\left(\frac{d^2z}{dt^2}\right)^n \approx \frac{2z^n - 5z^{n-1} + 4z^{n-2} - z^{n-3}}{(\Delta t)^2} \quad (4)$$

where z is the axial displacement and Δt is the time step. Combining Eq. 7 and Eq. 8, the displacement at time step n can be approximated:

$$z^n \approx \frac{(\Delta t)^2 \sum {F_z}^n}{2m} + \frac{5}{2}z^{n-1} - 2z^{n-2} + \frac{1}{2}z^{n-3}$$

$$\zeta^n = \begin{cases} z^n, & n = 0 \\ \alpha\, z^n + (1-\alpha)\, \zeta^{n-1}, & n > 0 \end{cases} \quad (5)$$

Finally, to ensure stable coupling between the solver and the jellyfish displacement, we used an exponentially-weighted moving average to smoothen the raw displacement z^n:

where ζ is the smoothed displacement prescribed to the jellyfish and $\alpha \in [0, 1]$ is the smoothing factor. We found $\alpha = 0.25$ was required for a robust simulation.

Verification and validation studies were performed to ensure the numerical and physical accuracy of our simulation. We first checked the sensitivity of our results to mesh and time step refinement (Fig. S4). A base mesh of 60895 cells (64 and 58 cell faces on the top and bottom bell contours, respectively) was refined to 135765 cells (86 and 82 cell faces on the top and bottom bell contours, respectively) and showed that the sum of forces acting on the jellyfish, and consequently its swimming performance, were insensitive to spatial refinement. Similarly, simulations run using a time step refined from Δt = 1/90 s to Δt = 1/180 s resulted in no appreciable change in the hydrodynamic forces acting on the jellyfish. Next, the instantaneous displacement of the numerical jellyfish was compared to the natural jellyfish used for the swimming kinematics (Fig. S5). Both show similar trends and indicate similar velocities throughout the swimming period, resulting in a nearly identical total displacement.

References.

1. Kim D & Gharib M (2011) Characteristics of vortex formation and thrust performance in drag-based paddling propulsion. *The Journal of Experimental Biology* 214(13):2283-2291.
2. Colin SP, *et al.* (2012) Biomimetic and Live Medusae Reveal the Mechanistic Advantages of a Flexible Bell Margin. *PLoS ONE* 7(11):e48909.
3. Linden PF & Turner JS (2004) 'Optimal' vortex rings and aquatic propulsion mechanisms. *Proceedings of the Royal Society of London. Series B: Biological Sciences* 271(1539):647-653.
4. Colin SP & Costello JH (2002) Morphology, swimming performance and propulsive mode of six co-occurring hydromedusae. *Journal of Experimental Biology* 205(3):427-437.

5. Dabiri JO, Colin SP, Katija K, & Costello JH (2010) A wake-based correlate of swimming performance and foraging behavior in seven co-occurring jellyfish species. *The Journal of Experimental Biology* 213(8):1217-1225.

6. Sutherland KR & Madin LP (2010) Comparative jet wake structure and swimming performance of salps. *The Journal of Experimental Biology* 213(17):2967-2975.

7. Ford MD & Costello JH (2000) Kinematic comparison of bell contraction by four species of hydromedusae. *Scientia Marina* 64:47-53.

8. O'Dor RK & Webber DM (1986) The constraints on cephalopods: why squid aren't fish. *Canadian Journal of Zoology* 64(8):1591-1605.

9. Webb PW, Kostecki PT, & Stevens ED (1984) The effect of size and swimming speed on locomotor kinematics of rainbow trout. *Journal of Experimental Biology* 109(1):77-95.

10. Videler JJ & Hess F (1984) Fast continuous swimming of two pelagic predators, saithe (*Pollachius virens*) and mackerel (*Scomber scombrus*): a kinematic analysis. *Journal of Experimental Biology* 109(1):209-228.

11. Dabiri JO, Colin SP, Costello JH, & Gharib M (2005) Flow patterns generated by oblate medusan jellyfish: field measurements and laboratory analyses. *The Journal of Experimental Biology* 208(7):1257-1265.

12. Larson RJ (1987) Costs of transport for the scyphomedusa Stomolophus meleagris L. Agassiz. *Canadian Journal of Zoology* 65(11):2690-2695.

13. Acuña JL, López-Urrutia Á, & Colin S (2011) Faking Giants: The Evolution of High Prey Clearance Rates in Jellyfishes. *Science* 333(6049):1627-1629.

14. Bone Q & Trueman ER (1983) Jet propulsion in salps (Tunicata: Thaliacea). *Journal of Zoology* 201(4):481-506.

15. Bone Q (1978) *Locomotor muscle* (London: Academic Press., New York) pp 361–424

16. Costello JH, Colin SP, & Dabiri JO (2008) Medusan morphospace: phylogenetic constraints, biomechanical solutions, and ecological consequences. *Invertebrate Biology* 127(3):265-290.

17. Dabiri JO, Colin SP, & Costello JH (2007) Morphological diversity of medusan lineages constrained by animal–fluid interactions. *Journal of Experimental Biology* 210(11):1868-1873.

18. Sahin M, Mohseni K, & Colin SP (2009) The numerical comparison of flow patterns and propulsive performances for the hydromedusae Sarsia tubulosa and Aequorea victoria. *Journal of Experimental Biology* 212(16):2656-2667.

19. Alexander RM (1964) Visco-elastic properties of the mesogloea of jellyfish. *Journal of Experimental Biology* 41(2):363-369.

20. Demont ME & Gosline JM (1988) Mechanics of Jet Propulsion in the Hydromedusan Jellyfish, Polyorchis Penicillatus: II. Energetics of the Jet Cycle. *Journal of Experimental Biology* 134(1):333-345.

21. Demont ME & Gosline JM (1988) Mechanics of Jet Propulsion in the Hydromedusan Jellyfish, Polyorchis Pexicillatus: I. Mechanical Properties of the Locomotor Structure. *Journal of Experimental Biology* 134(1):313-332.

22. Megill WM, Gosline JM, & Blake RW (2005) The modulus of elasticity of fibrillin-containing elastic fibres in the mesoglea of the hydromedusa Polyorchis penicillatus. *Journal of Experimental Biology* 208(20):3819-3834.

23. Dickinson MH & Lighton JR (1995) Muscle efficiency and elastic storage in the flight motor of Drosophila. *Science (New York, N.Y.)* 268(5207):87-90.

24. Lipinski D & Mohseni K (2009) Flow structures and fluid transport for the hydromedusae Sarsia tubulosa and Aequorea victoria. *The Journal of Experimental Biology* 212(15):2436-2447.

25. Steinhausen M, Steffensen J, & Andersen N (2005) Tail beat frequency as a predictor of swimming speed and oxygen consumption of saithe (Pollachius virens) and whiting (Merlangius merlangus) during forced swimming. *Marine Biology* 148(1):197-204.

26. Lynam CP, *et al.* (2006) Jellyfish overtake fish in a heavily fished ecosystem. *Current Biology* 16(13):492.

27. Martin LE (2001) Limitations on the Use of Impermeable Mesocosms for Ecological Experiments Involving Aurelia sp. (Scyphozoa: Semaeostomeae). *Journal of Plankton Research* 23(1):1-10.

28. McHenry MJ & Jed J (2003) The ontogenetic scaling of hydrodynamics and swimming performance in jellyfish (Aurelia aurita). *J Exp Biol* 206(Pt 22):4125-4137.

29. Uye S & Shimauchi H (2005) Population biomass, feeding, respiration and growth rates, and carbon budget of the scyphomedusa Aurelia aurita in the Inland Sea of Japan. *Journal of Plankton Research* 27(3):237-248.

30. Schmidt-Nielsen K (1972) Locomotion: energy cost of swimming, flying, and running. *Science* 177(4045):222-228.

31. Brett JR & Glass NR (1973) Metabolic Rates and Critical Swimming Speeds of Sockeye Salmon (Oncorhynchus nerka) in Relation to Size and Temperature. *Journal of the Fisheries Research Board of Canada* 30(3):379-387.

32. Larson RJ (1987) Trophic ecology of planktonic gelatinous predators in Saanich Inlet, British Columbia: diets and prey selection. *Journal of Plankton Research* 9(5):811-820.

Acknowledgments:

New England Aquarium provided cultured medusae. BG, JHC, SPC, CS, DT and SP were supported from the MURI grant through the Office of Naval Research (N00014-08-1-0654), JOD (N00014-10-1-0137).

Figures:

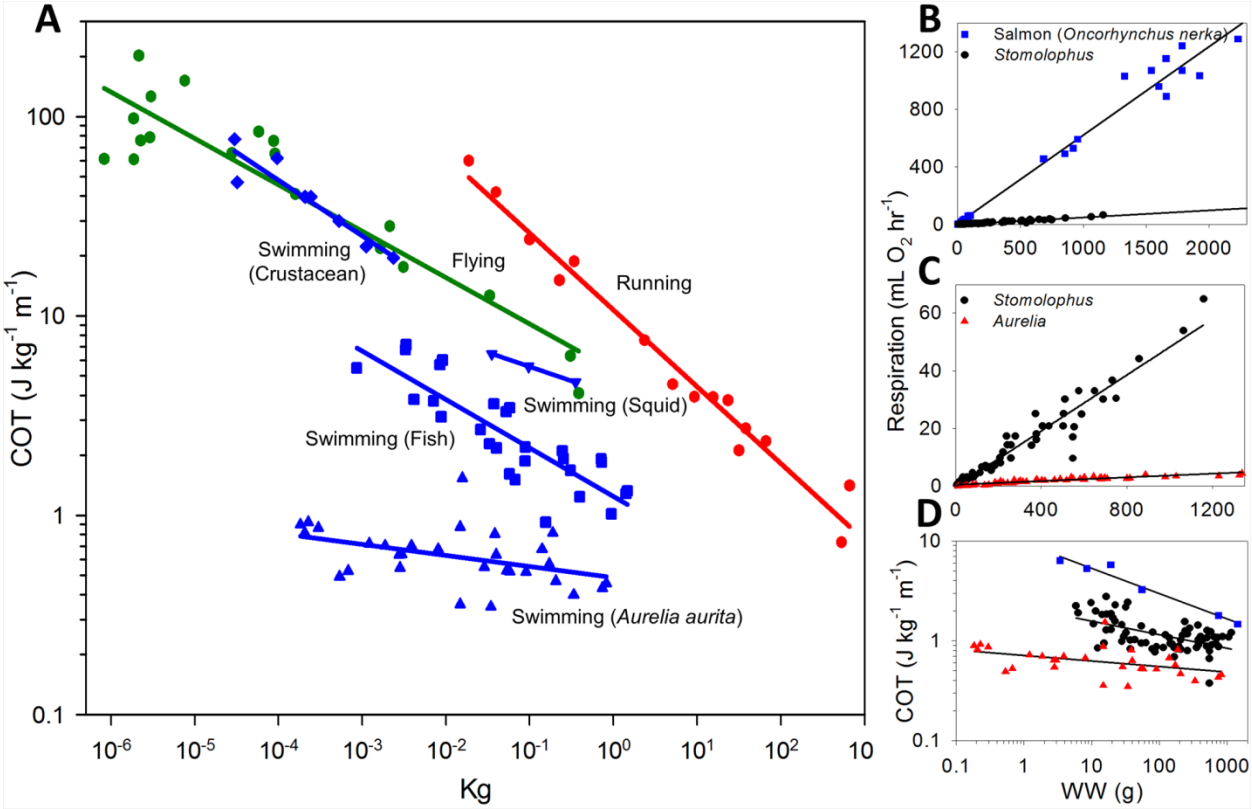

Figure 1. Energetic swimming comparisons of propulsive modes. A) Net cost of transport (COT) based on wet-mass. Data for fliers and runners are re-plotted from (30). Crustaceans and squid are re-plotted from (12). Fish data was combined from both (12, 30). Data for *Aurelia aurita* was calculated with swimming speed vs body size from the current study and supplemented with data from (27, 28), and metabolic data from (29). B) Net respiration rates of locomotion for the salmon (*Oncorhynchus nerka*) and a rhizostome jellyfish (*Stomolophus meleagris*). C) Net respiration rates of locomotion for *S. meleagris* and *A. aurita*. D) Net cost of transport (COT) for all 3 species. Data used for respiration and COT in salmon was obtained from (31) and *Stomolophus* data was re-plotted from (32).

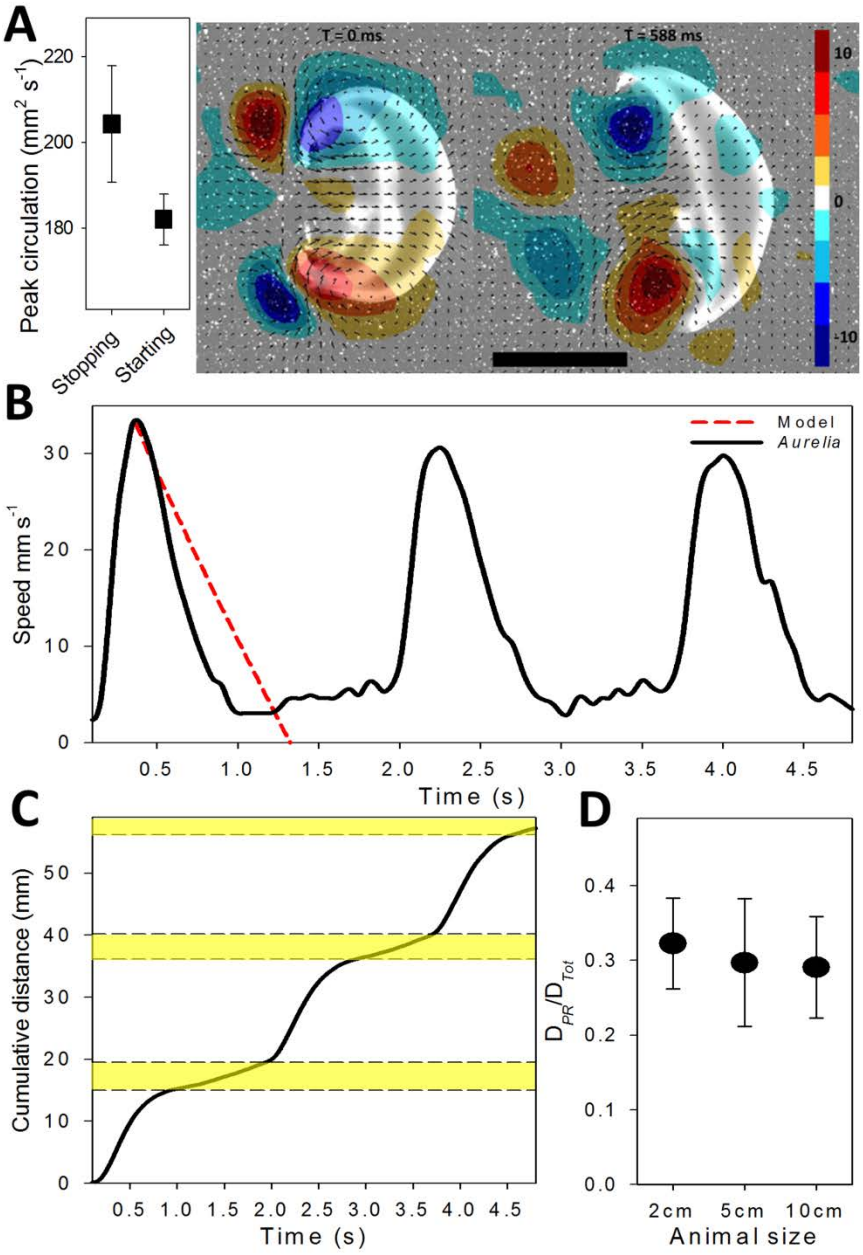

Figure 2. Swimming performance of *Aurelia aurita*. Maximum circulation and vorticity starting and stopping vortices during normal swimming (cruising). Scale bar = 1cm. B) Representative swimming sequence of a 3cm *A. aurita*, showing an increase in speed during periods of no kinematic body motion (post recovery). The model (red) shows a conservative estimate of the change in speed with time from inertia alone. C) The cumulative distance of the jellyfish shown in panel B. Yellow represents distance gained from passive energy recapture. D) Effect of passive energy recapture with size (bell diameter). No difference (P = 0.550) is observed among body size and the relationship between distance travelled from passive energy recapture (D_{PR}) relative to the total distance travelled per swimming stroke (D_{Tot}).

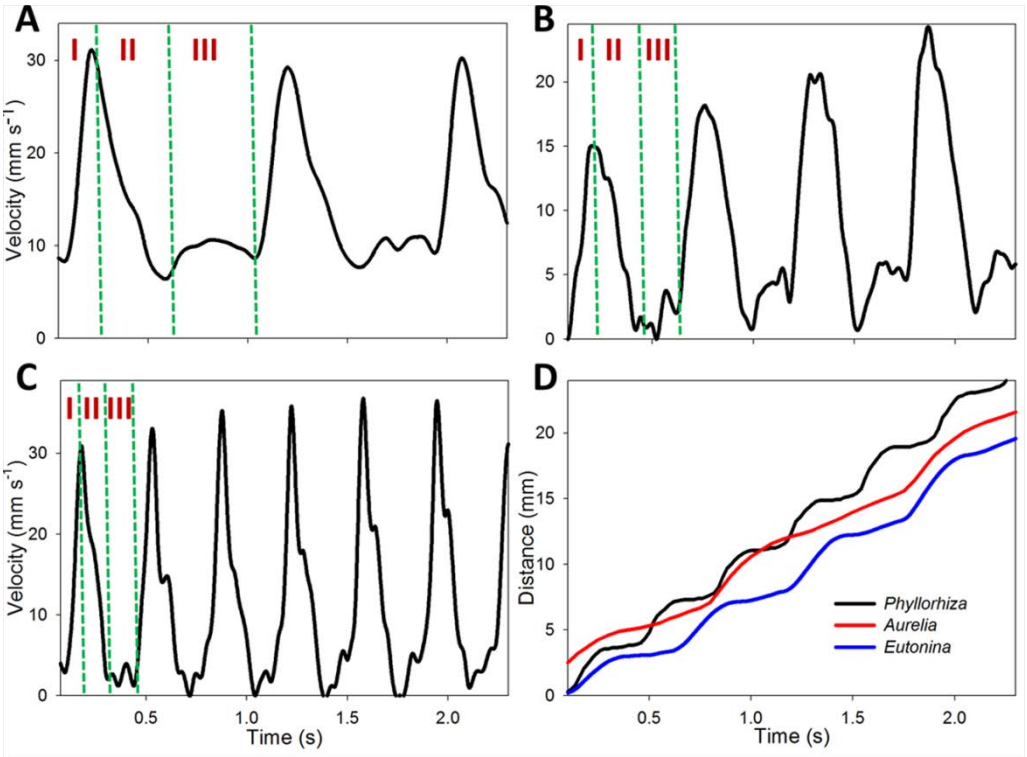

Figure 3. Swimming performance for 3 species of jellyfish, showing species variation in the durations of contraction (I), Relaxation/refilling (II) and the inter-pulse duration during which thrust from passive energy recapture occurs (III). All 3 species exhibit enhanced thrust during this third phase. A) An oblate scyphomedusae, *Aurelia aurita*. B) A hydromedusae, *Eutonina indicans*. C) A rhizostome, *Phyllorhiza punctata*. D) Cumulative swimming distance for all 3 species.

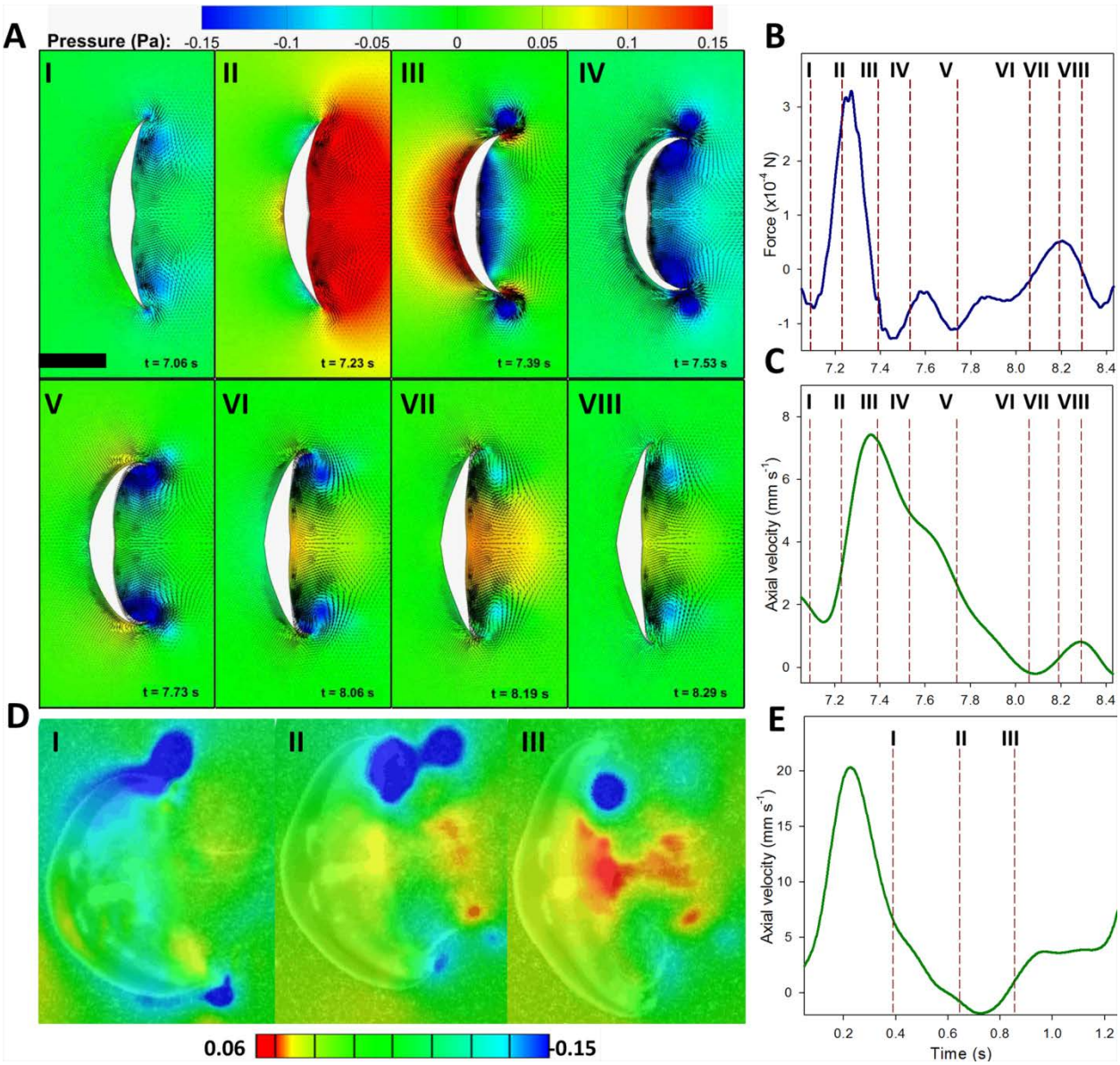

Figure 4. Computational fluid dynamics (CFD) of a 3 cm swimming *Aurelia aurita*. A) Pressure around the body during a swimming cycle. Note the secondary increase in pressure at the subumbrellar surface (Panel VI-VIII) and resulting axial force and boost in velocity. B) Axial force showing the corresponding locations from panel A. A secondary peak corresponding to positive pressure of the induced flow created by the stopping vortex accumulating against the subumbrellar surface. C) Velocity-time plot showing the corresponding locations from panel A. D) Results from an empirically based technique for pressure estimation from velocity field measurements around a 3.5 cm *A. aurita*. E) Velocity-time plot showing the corresponding locations from panel D.